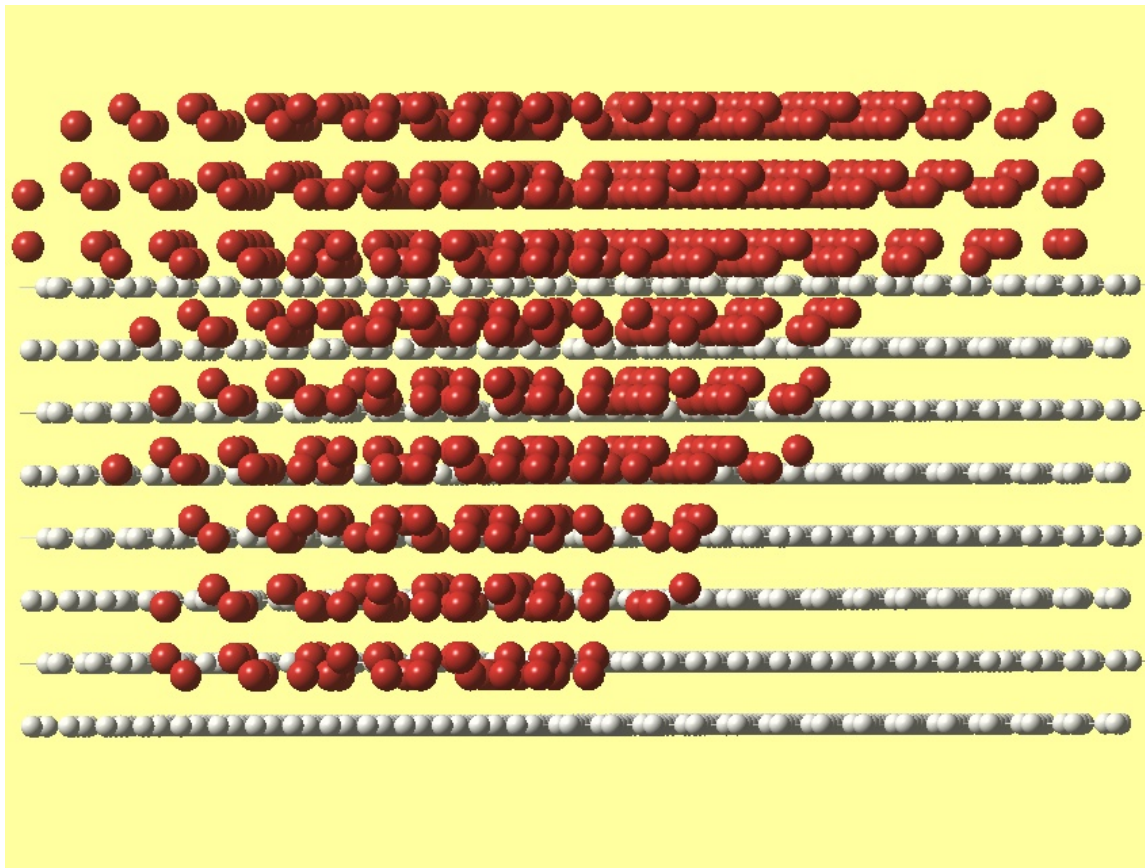


Part III

Surface Assemblies and Interfacial Phenomena

Chapter 9

Ordered Water Structure and Its Dynamics at Hydrophobic Graphite Interfaces[†]



[†]adapted from D.-S. Yang, A. H. Zewail, *Proc. Natl. Acad. Sci. USA* **106**, XXXX (2009).

Introduction

Water at interfaces is fundamental to the understanding of various phenomena, such as wetting, molecular recognition and macromolecular folding. When compared with bulk phases (*1, 2*), the nanometer-scale interface is believed to have a unique function in nanotribology (*3, 4*), chemical reactivity (*4-6*) and biological structure and dynamics (*7-10*). From the structural point of view, considering the energetics, the determining factor at interfaces is the delicate balance of hydrogen bonding among water molecules and the comparable interactions with a substance, defining the two extremes of hydrophobic and hydrophilic behavior. However, the time scales of structural dynamics are important for defining the microscopic mechanisms of relaxations and the role of substrate structure and morphology (*11*). For water ice on a hydrophilic substrate, the ordered layers are evidenced by their diffraction (Bragg spots), and this long-range order is lost when the ice assembly becomes at a distance from the substrate (*12*). On hydrophobic surfaces, the expected picture is that randomly oriented crystallites form with no interfacial long-range order, because of the stronger intermolecular interactions when compared with those of water–substrate.

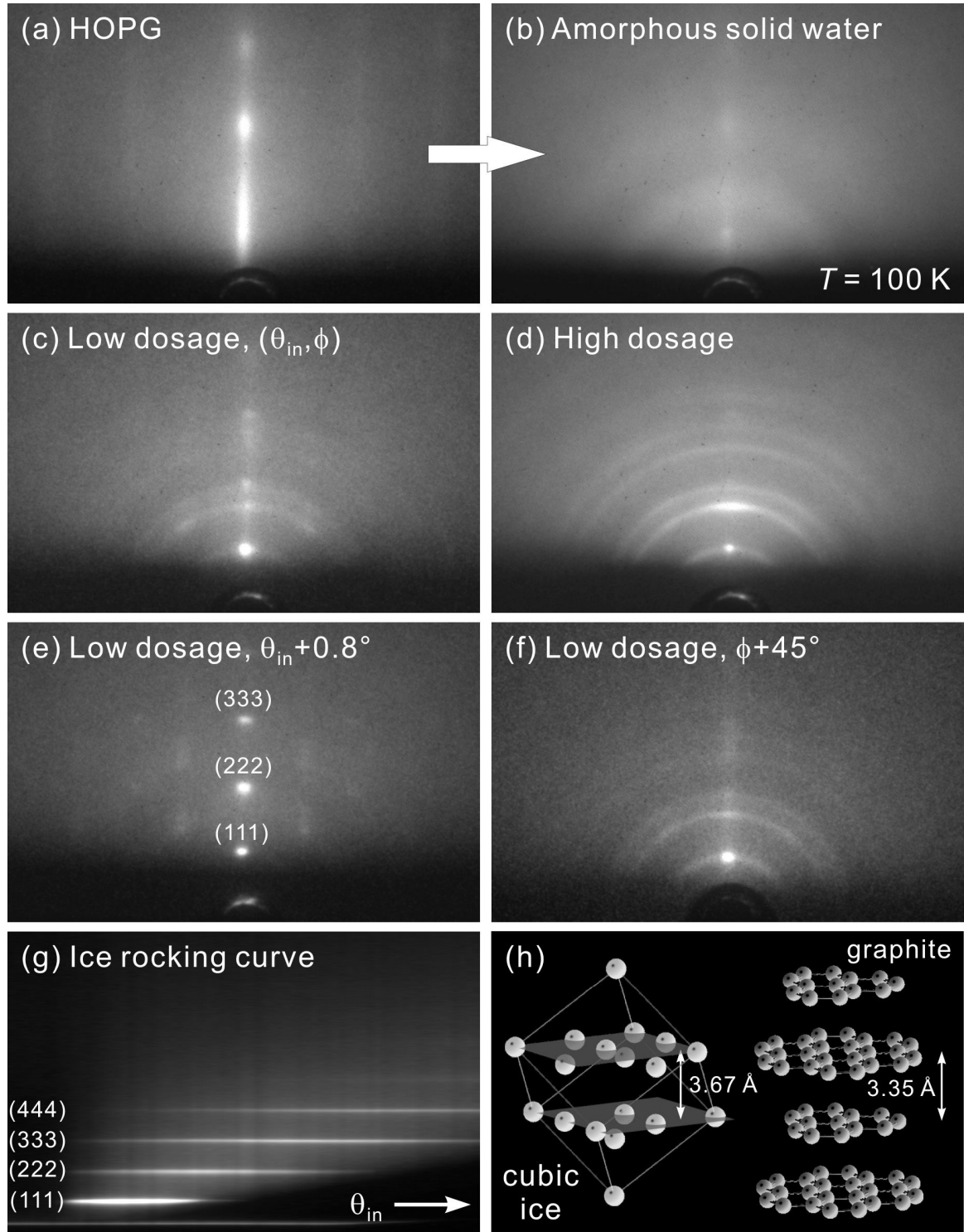
In this chapter, I describe the determination of the structure and dynamical behavior of a water assembly on highly oriented pyrolytic graphite (HOPG), a hydrophobic substrate. Through diffraction, ultrafast electron crystallography (UEC) provides the position of atomic planes and the temporal change of the structure. Electron crystallography (*13*), because of the large electron scattering cross section, is ideal for these surface and interface probings. Here, it is shown that the layered structure of HOPG serves as a substrate and promotes the crystalline order in the ice thin film along the surface normal direction. Upon heating the substrate by an infrared femtosecond pulse,

the interfacial ice assembly goes through nonequilibrium phase transformation, into a highly expanded lattice, a dynamical behavior evidenced by the appearance of a “structural isosbestic point” in the diffraction profiles. The ice “melting” time is 10 ps and the new phase grows in 20 ps, whereas the restructuring time is significantly longer, being 75 and 390 ps. From the intense Bragg (spot) diffraction, it is concluded that ice on hydrophobic graphite has a high degree of order on the nanometer scale (and also in the expanded state) similar to that reported on a hydrophilic substrate (12). This finding suggests the important role of surface morphology.

Materials and Experimental Section

The HOPG substrate, which was obtained from Structure Probe, Inc. (grade 1), was cleaved and immediately mounted on the goniometer inside the diffraction chamber; an ultrahigh vacuum of $\sim 10^{-10}$ torr at low temperature was maintained during the experiment. To prepare the interfacial water assembly, the goniometer was first cooled down to $T = 100$ K by a constant flow of liquid nitrogen, and the flow rate was decreased to achieve a higher temperature when necessary. At 3 cm above the substrate, molecules of water (NANOpure, resistivity $> 18.0 \text{ M}\Omega\cdot\text{cm}$) were effused through a micrometer-sized pinhole of a doser system containing only saturated water vapor (~ 20 Torr) at room temperature (12). The extent of water layer deposition was controlled by the dose time. The amorphous solid water initially deposited on HOPG at $T = 100$ K begins to transform into a polycrystalline assembly of the cubic-ice structure at $T \sim 135$ K, with a preference of vertical stacking of (111) bilayers but no horizontal orientation order.

The time-resolved experiments were carried out after the deposited interfacial water was thermally crystallized (annealed) and then maintained at $T = 100$ K. We used



(See next page for the figure caption.)

Fig. 1. Diffraction patterns of ice on hydrophobic graphite at various conditions.

(a) Diffraction pattern of a freshly cleaved HOPG surface. The grazing incidence and nanometer depth of electron probing give rise to the rod-like pattern. (b) Diffraction pattern at the same probing condition as panel a after the deposition of water molecules at a surface temperature of $T = 100$ K. The diffuse scattering without distinct diffraction features indicates that the water assembly is in an amorphous state. (c) Diffraction pattern from a thin interfacial water layer after its crystallization into an ice assembly through thermal annealing. The most distinct diffraction feature is the intense Bragg spot at the center, signifying an ordered structure along the surface normal direction. (d) The pattern from a thicker ice assembly at the same probing condition as panel c. While the central Bragg spot is still apparent, a Debye–Scherrer ring pattern becomes clearly evident, indicating that the ice crystallites away from the substrate surface are randomly oriented. (e) The pattern from a thin ice assembly at a larger incidence angle ($\theta_{in} + 0.8^\circ$). Higher orders of the original (111) Bragg spot are now apparent. (f) The pattern from a thin ice assembly at a different azimuthal angle ($\phi + 45^\circ$) by rotating the substrate. From such an azimuthal search, the lack of other spots except for the original central one reflects the lack of a horizontal orientation order in the ice structure. (g) Rocking curve for a thin ice assembly obtained by collecting the central rod area of diffraction patterns as a function of θ_{in} . The equally spaced streaks are indicative of ordered vertical stacking of ice bilayers. (h) Structures of cubic ice (hydrogen atoms are omitted) and graphite.

120-fs near-infrared pulses (800 nm) to induce the substrate temperature (T) jump; at this wavelength and adsorbate thickness there is no absorption in the ice layers. The electron diffraction patterns were recorded for different delay times between the optical and electron pulses, with a grazing electron incidence angle of $\theta_{in} \sim 0.6^\circ$. The optical excitation fluence used was up to 39 mJ/cm^2 at the peak. The scheme of pulse front tilting (14–17), which enables femtosecond resolution, was not employed because, in the case discussed here, the doser system for water deposition was connected on top of the chamber and the temporal resolution (capable of detecting 2-ps change; 7 ps in total) was sufficient for the dynamics. The ice–substrate composite was fully recovered in less than 1 ms without noticeable water sublimation, as evidenced by the reproducibility of the diffraction pattern at negative times and for our experimental repetition rate of 1 kHz.

Results and Discussion

In Fig. 1, the diffraction patterns obtained in the absence of the T -jump are displayed. The bare substrate shows an intense, intensity-modulated diffraction rod in the center and faint ones on the sides, indicating the regular vertical stacking of graphite sheets and the lack of long-range (micrometer-scale) horizontal orientation (Fig. 1a). With water molecules immobilized on the surface at $T = 100 \text{ K}$, the graphite pattern becomes weaker and is replaced by diffuse scattering from the initially formed amorphous phase (Fig. 1b); its thickness, depending on dose time, is on the order of 10 nm, which was estimated from the electron penetration depth at 30 keV. Crystallization of the amorphous film begins at $\sim 135 \text{ K}$, which is close to the reported transition temperature (1, 2). Completion of crystallization occurs at about 145–150 K, and total sublimation at near 150–160 K, both depending on the film thickness.

The crystallized ice layers show intriguing diffraction patterns. For smaller thickness layers, an intense Bragg spot appears at the middle of the first Debye–Scherrer ring, together with a weak ring pattern that indicates the existence of some randomly oriented ice crystallites (Fig. 1c). Higher orders of this intense Bragg spot can be seen in the rocking curve at larger incidence angles, θ_{in} (Fig. 1, panels e and g). No other spots can be found during the azimuthal rotation (ϕ) of the substrate (Fig. 1f), which reflects the lack of a horizontal orientation order in the ice assembly (Ch. 2). For a thicker layer structure, the diffraction ring pattern intensifies and the aforementioned Bragg spot on the first ring, although less intense, is still apparent (Fig. 1d). These results are in sharp contrast with the many-spot pattern observed from the ordered crystalline ice on a hydrophilic surface (12), and with the pure ring pattern observed from the randomly oriented polycrystalline ice on other hydrophobic surfaces, such as hydrogen-terminated silicon (Ch. 10), or when water is away from the surface (12).

In order to determine the structure of ice, radial averaging of the diffraction rings was made. The one-dimensional diffraction intensity profile, with its distinct peaks, matches well with the theoretically derived profile of the cubic-ice structure *Ic*, giving a lattice constant of $a = 6.36 \text{ \AA}$; the hexagonal structure *Ih* was excluded because of its different pattern (12). The enhancement of rings in diffraction from a thicker adsorbate indicates that the randomly oriented ice *Ic* crystallites are in the upper part of the ice assembly, away from the influence of the substrate. However, near the graphite surface water molecules form an ordered structure. A Bragg spot in the center on the (111) ring was observed without other spots on other rings. This uniquely intense spot signifies that the (111) planes of ice are stacked with order in parallel with the substrate planes (001), but without an azimuthal long-range order. In this configuration, for the (111) planes of

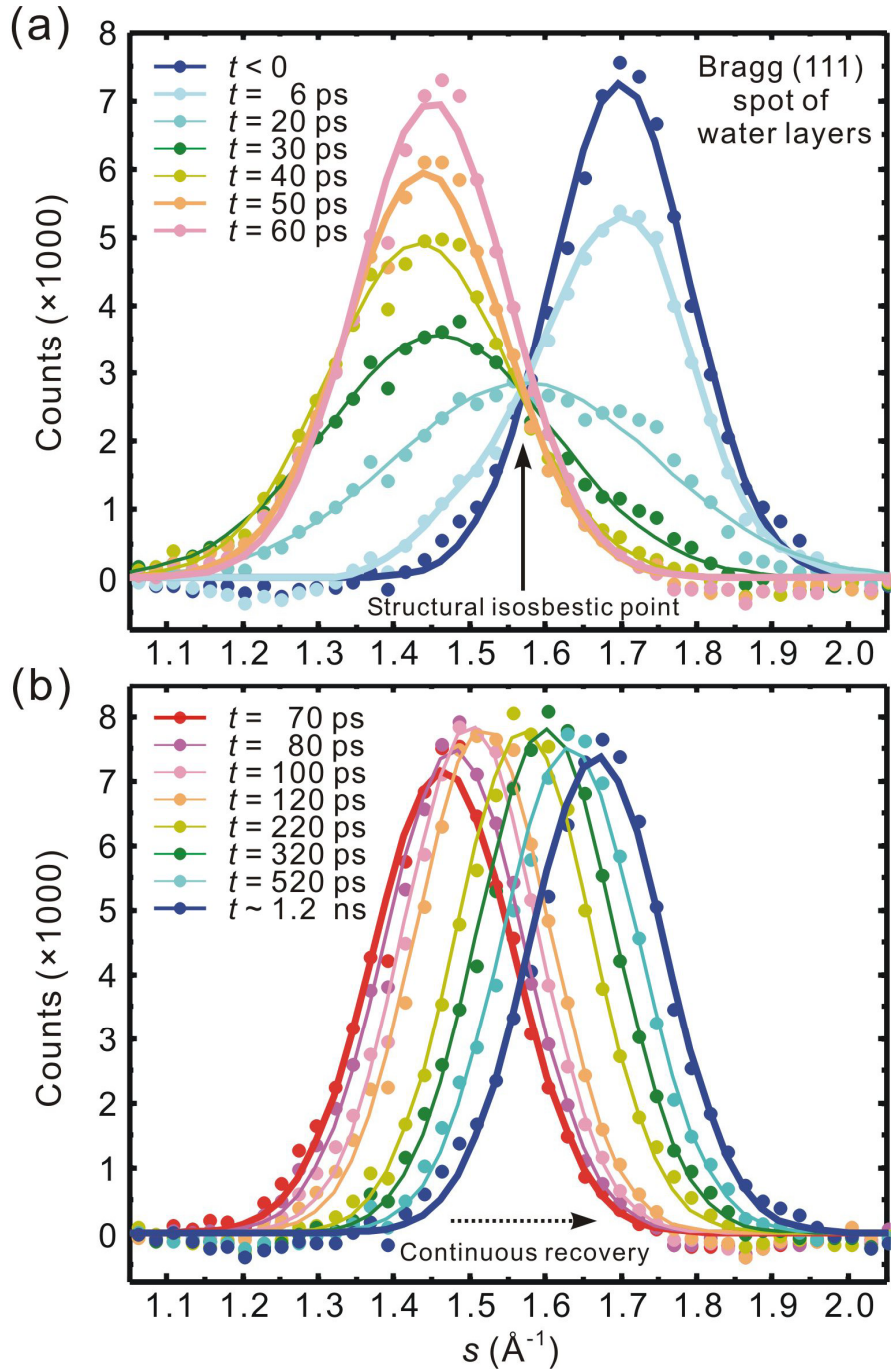


Fig. 2. Diffraction vertical profiles at different times. Shown are the family of curves for the (111) Bragg spot of interfacial ice on graphite, at (a) early times and (b) longer times. The initial peak fluence for graphite T -jump is 24 mJ/cm^2 . It is noted that the early-time dynamics displays a structural isosbestic point, whereas the longer-time behavior depicts a continuous profile shift toward the initial, ground-state structure.

cubic ice, the out-of-plane O–H bonds are perpendicular to the planes (see below).

Such an ordered conformation is possible because of the structural morphology of graphite. Layered HOPG is known to have a stepped structure and terraces (18). Also, the interplanar distance ($a/\sqrt{3} = 3.67 \text{ \AA}$) between (111) planes of cubic ice and that between the sheets of HOPG (3.35 Å) are comparable within 10% (Fig. 1h). Molecular dynamics simulations have suggested that, even at a higher temperature, water molecules in contact with graphite tend to project some hydrogen atoms toward the surface (19, 20), a preference that is compatible with the stacking of (111) planes of ice *Ic*. Therefore, the HOPG substrate becomes a confinement template for structural ordering of the interfacial assembly, even though water–graphite interactions are somewhat weaker than those of water–water in the network. Random orientation of ice crystallites resumes when such influence is attenuated at a distance away from the substrate.

For studies of ice dynamics, we focus on the (111) Bragg spot under the condition given in Fig. 1c, at low dosage and small θ_{in} of 0.6°; under such conditions, the (111) specular diffraction is the most prominent. It was found that the spot exhibits a large vertical-only movement with unique intensity change as a function of time. In Fig. 2, vertical profiles of the diffraction spot at different delay times t are displayed. Initially, the diffraction spot is located at $s = 1.71 \text{ \AA}^{-1}$, where the momentum transfer value $s = (4\pi/\lambda)\sin(\theta/2)$, the de Broglie wavelength $\lambda = 0.07 \text{ \AA}$ at 30 keV, and θ is the total scattering angle. Immediately after the substrate is heated, the (111) Bragg spot intensity decreases, followed by a profile transformation to a new position at $s = 1.45 \text{ \AA}^{-1}$. This change in s corresponds to an 18% increase in the (111) water bilayer separation. The huge change was unexpected, but equally surprising was the crossing of all curves at the same point (a structural isosbestic point) in the middle with $s = 1.57 \text{ \AA}^{-1}$ (Fig. 2a,

$t = 6$ to 50 ps). After the transformation, the diffraction intensity recovers and the peak position continuously shifts (not through the isosbestic point) toward the original equilibrium value (Fig. 2b). The clear difference in the evolution of the diffraction curves at early and later times is easy to discern.

The appearance of a structural isosbestic point at early times signifies that the initial conversion involves two distinct states, the untransformed ground-state ice structure and a transformed, expanded one. In spectroscopic studies, the appearance of an isosbestic point in the spectra as evidence for interconverting chemical or structural species has been called into question (21, 22). However, the main problem there is the presence of inhomogeneous broadenings. In diffraction, the well-defined Bragg spots can only originate from a long-range ordered (homogeneous) structure. Moreover, the clear shift of the diffraction peak during the early-time dynamics, with the existence of only one isosbestic point and no overlap in the wings, is in sharp contrast with the results given in Ref. 21. In fact, the well-separated peaks before time zero and after 50 ps demarcate the two distinct structures involved, each with a well-defined diffraction peak width. Moreover, as suggested in Ref. 21, the confirmation of a true chemical or structural conversion must come from time-dependent measurements, as reported here using diffraction.

Therefore, it was legitimate to fit the early-time diffraction profile to two Gaussian peaks centered at $s = 1.71 \text{ \AA}^{-1}$ and 1.45 \AA^{-1} , with variable intensities but having a width similar to the ground-state value of $\sim 0.20 \text{ \AA}^{-1}$. The width of a diffraction peak is determined by the size of the electron beam (a constant value), the broadening effect described by the Scherrer formula due to the finite size of ordered structure (Eq. 23 of Ch. 2), and electron refraction due to the shape of the crystallites (see Chs. 2 and 5).

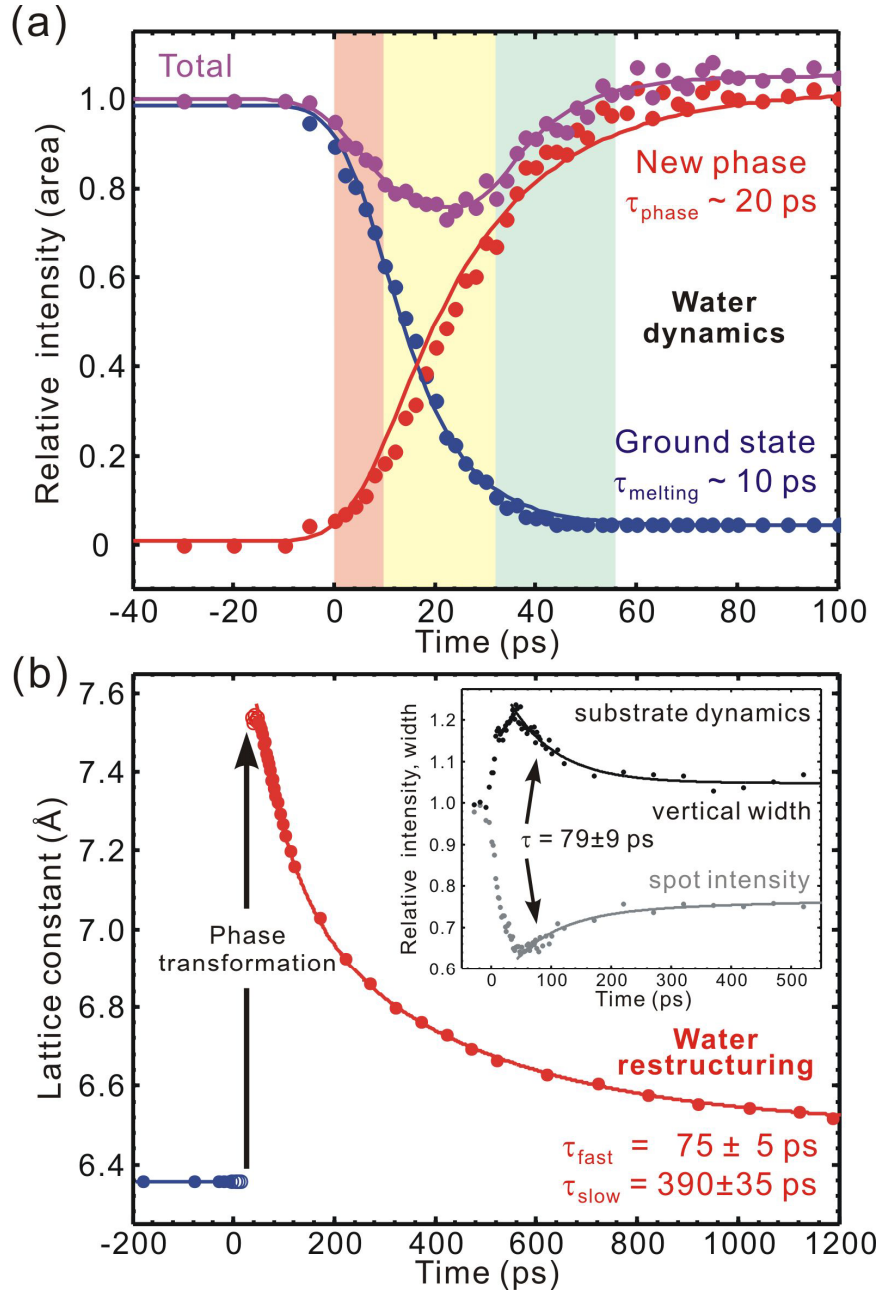


Fig. 3. Evolution of the collective phase and its restructuring to the ground state.

(a) Depletion of the ground-state ice structure and growth of the new phase, together with the sum of their proportions. Three sequential stages are noted for the dynamics, from left to right in different colors: ultrafast melting, nonequilibrium phase transformation, and structural annealing. (b) Restructuring of the expanded lattice at longer times. Inset: Temporal evolution of the intensity and width of the (004) spot of graphite.

During a nonequilibrium phase transformation, the latter two factors, in principle, do not change significantly, leading the width for each Gaussian profile to remain similar to that of the ground-state. The temporal evolution of the intensity of each component and their sum, relative to the unperturbed value at negative times, is shown in Fig. 3a. It follows from the plot that the ground-state structure disappears with a time constant of $\tau_{\text{melting}} \sim 10$ ps, and the new phase grows with a time constant of $\tau_{\text{phase}} \sim 20$ ps. The total intensity, as described earlier, shows a relatively small decrease following time zero, but maintains a constant value, which is supportive evidence for structural phase transformation; the initial and final states of the conversion have the same electron diffraction cross section as both contain oxygen and hydrogen.

Unlike the structural phase transition observed in charge-induced correlated solids (Ch. 7), the behavior in the present case of the ice–graphite composite is the result of collective structural expansion and across-interface energy transfer. The lattice of graphite has been shown to undergo an interlayer contraction followed by a large expansion with a time constant of ~ 7 ps (15). The “old-structure” disappearance time τ_{melting} for ice given here matches well with the convolution of the 7-ps time for graphite with the instrumental response, indicating that the breakage of the original assembly conformation is due to the vibrational coupling of ice with underlying graphite. It is noted that, after time zero, the energy deposited induces large-amplitude motion which results in diffraction intensity to decrease by $\sim 20\%$ (Fig. 3a, purple). We estimate a vertical vibrational amplitude of $\langle \delta u_z^2 \rangle^{1/2} \sim 0.28$ Å for oxygen atoms, using the Debye–Waller factor (Eq. 16 of Ch. 2).

In order to accommodate such a large structural perturbation and the undulating substrate, the stack of (111) water bilayers expands collectively, similar to a phase

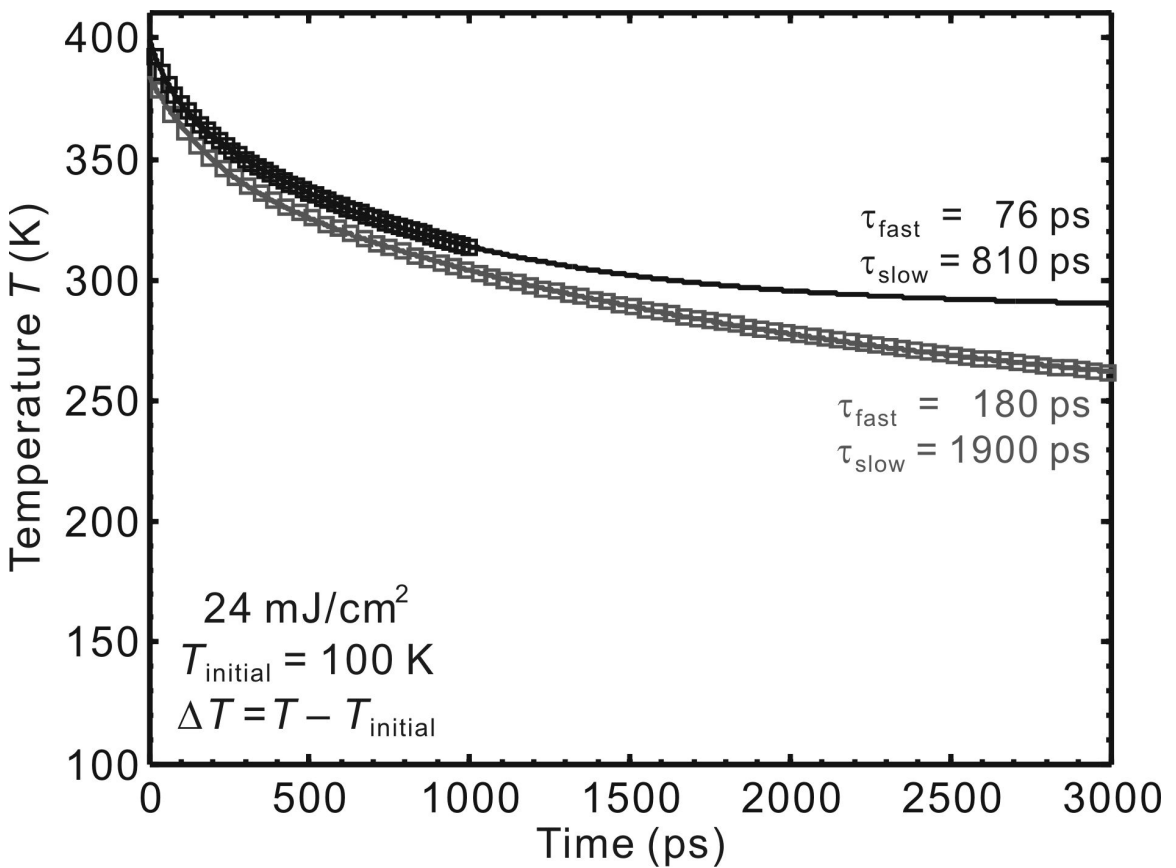


Fig. 4. One-dimensional heat diffusion in the substrate (graphite). Shown is the temperature change as a function of time considering two temporal ranges, up to 1 ns and 3 ns. The following values were used in the simulation: the full fluence of 24 mJ/cm^2 , reflectivity of $\sim 30\%$, heat capacity of $1.33 \text{ J g}^{-1} \text{ K}^{-1}$ at the substrate initial temperature of 100 K (37), density of 2.266 g/cm^3 , thermal conductivity of $0.157 \text{ W cm}^{-1} \text{ K}^{-1}$ at 100 K (37), and penetration depth of 187 nm at the excitation wavelength of 800 nm (38). We note that the derived time constants are affected by the time range but the profiles are robust; see Text for discussion of the asymptotic value. The top trace is shifted by 10 K for clarity.

transformation, with a rise time τ_{phase} . It is noted that connectivity in the network of hydrogen bonds prevents the sublimation of ice, even though the large expansion motion (23) seems to exceed the equilibrium Lindemann limit for thermal melting, i.e., when the root-mean-square amplitude of thermal vibration exceeds $\sim 10\%$ of the nearest-neighbor distance. With time, the amplitude buildup of the substrate atomic motions comes to an end, and this is reached when a plateau in the intensity and vertical width is experimentally realized (Fig. 3b, inset; see also Ch. 2).

When this state of mature phase formation is reached, the transformed ice structure behaves collectively and begins its recovery as a unit. At these time scales, the diffraction curves can be fitted to a single Gaussian profile. From the observed shifts at different times, we obtained the lattice constants given in Fig. 3b. The expanded ice lattice is seen to restructure continually to the ground-state structure with two apparent time constants, $\tau_{\text{fast}} = 75 \pm 5$ ps and $\tau_{\text{slow}} = 390 \pm 35$ ps. In Fig. 4, we present calculations of the temperature versus time using the one-dimensional heat diffusion equation (Eq. 2 of Ch. 4), considering the fluence of the laser pulse and the initial temperature of graphite (100 K). The temporal behavior exhibits apparent biexponential decay, but the time constants extracted depend on the range of time delay during which the data are obtained; our time range is 1.2 ns and from the simulation, τ_{fast} and τ_{slow} become 76 and 810 ps, respectively. It is interesting to note that such a simple diffusion model reproduces the featured two exponentials, and that the fast component observed in ice matches that of graphite ($\tau_{\text{fast}} = 79 \pm 9$ ps in Fig. 3b, inset). Also, the asymptotic temperature at long times in Fig. 4 mirrors the behavior in graphite (Fig. 3b, inset) but for ice, the restructuring is close to 85% complete in 1.2 ns (Fig. 3b). These findings suggest that restructuring of ice is determined by heat dissipation in the substrate and that the exchange of energy

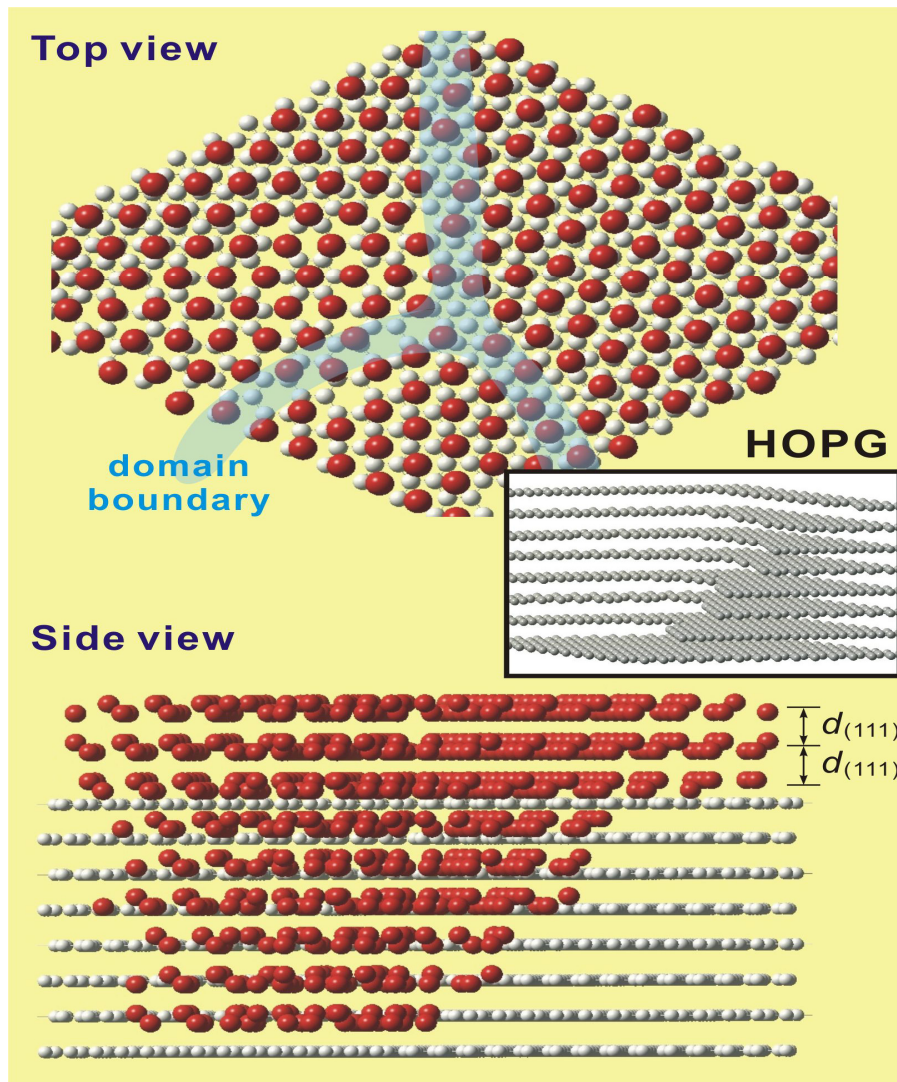


Fig. 5. Schematic representation of the structure for the water layers on hydrophobic graphite (HOPG). Oxygen atoms are in red, carbon in light grey, and hydrogen atoms are omitted for clarity. (Upper) Top view revealing the hexagonal arrangement of oxygen atoms in the (111) planes of cubic ice. Domains with different azimuthal orientations are depicted. (Lower) Side view showing the water bilayers stacked along the surface normal direction. The steps and terrace of HOPG, and the similarity in distance between water bilayers and graphite layers, lead to the observed vertical order. (Inset) Schematic of layered HOPG with an emphasis on its stepped structure. The many steps depicted in a small region are not drawn to scale.

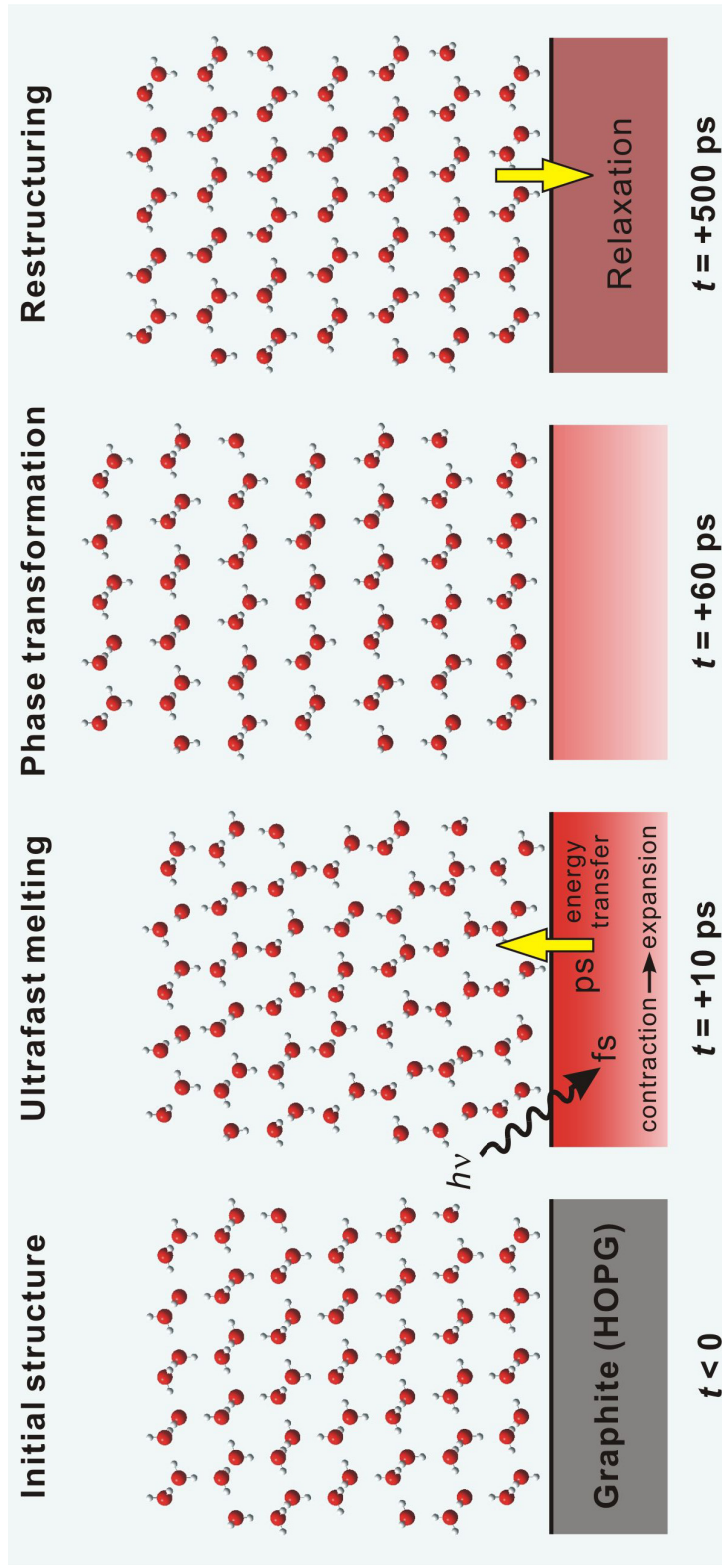


Fig. 6. Schematic representation of the dynamics for the ice layers on graphite. (Middle left) After the ultrafast heating initiated by an infrared light pulse, the substrate undergoes lattice contraction followed by expansion (15). The transfer of vibrational energy to the interfacial ice assembly leads to (partial) structural randomization in the first 10 ps. (Middle right) A collective structural motion in ice then takes place, which results in a nonequilibrium phase transformation into an expanded ice structure. (Right) On a longer time, energy transfer from ice to the substrate together with the relaxation of graphite itself establishes equilibration of the composite system; the ice structure subsequently returns to its original state.

between ice and the substrate is ultrafast both ways, i.e., there is no bottleneck in the adsorbate–substrate heating and cooling.

Conclusion

The observations by UEC unravel the unique nature of structure and dynamics of an interfacial water assembly on graphite, a hydrophobic substrate. In comparing the ordered behavior on graphite with the nonordered (long range) behavior on another hydrophobic surface, hydrogen-terminated silicon(111) (Ch. 10), it is concluded that surface morphology plays a direct role in stabilizing the ordered network on graphite, as schematically shown in Fig. 5. For ice on Pt(111), both the surface steps and screw dislocations are critical in the formation of metastable cubic structure (and not the hexagonal one) and in the growth (24).

Spectroscopic investigation of interfacial D₂O ice, using sum-frequency generation with longer time resolution, suggested the presence of melted regions, but neither the structure nor the order was possible to observe with atomic-scale resolutions (25). Unlike in conventional heating, the lack of sublimation of ice on the time scale reported here is due to ultrafast melting (or softening) in $\tau_{\text{melting}} \sim 10$ ps and restructuring in $\tau_{\text{fast}} = 75$ ps and $\tau_{\text{slow}} = 390$ ps (see Fig. 6), with the cooling being determined by substrate heat diffusion characteristic. These time scales are significantly different from those deduced in figure 3(b) of Ref. 25 for ice on CO/Pt(111) but the picture is valid.

The structural (nonequilibrium) expansion reported here may correlate with the large thermal expansion of confined water when compared with the bulk property reflected in an increased density at the interface (26). However, significant hindrance of hydrogen-bond mobility has serious consequences on relaxation in bulk (27, 28) and

especially at interfaces (12, 29). Clearly, studies of hydrophobic/hydrophilic properties at interfaces (30-32), and the contrast with bulk properties (33), are of interest in many fields, and diffraction methods provide the means for elucidating structures and dynamics at the nanometer scale during phase transformations (34-36).

References and Footnote:

1. P. G. Debenedetti, H. E. Stanley, *Phys. Today* **56**, 40 (2003).
2. C. A. Angell, *Science* **319**, 582 (2008).
3. M. Binggeli, C. M. Mate, *Appl. Phys. Lett.* **65**, 415 (1994).
4. M. A. Henderson, *Surf. Sci. Rep.* **46**, 5 (2002).
5. G. E. Brown *et al.*, *Chem. Rev.* **99**, 77 (1999).
6. G. E. Brown, *Science* **294**, 67 (2001).
7. K. Gawrisch *et al.*, *Biophys. J.* **61**, 1213 (1992).
8. G. M. Whitesides, P. W. Snyder, D. T. Moustakas, K. A. Mirica, in *Physical biology: From atoms to medicine*, A. H. Zewail, Ed. (Imperial College Press, London, 2008), pp. 189-215.
9. S. K. Pal, A. H. Zewail, *Chem. Rev.* **104**, 2099 (2004).
10. L. Y. Zhang *et al.*, *Proc. Natl. Acad. Sci. USA* **104**, 18461 (2007).
11. A. H. Zewail, *Annu. Rev. Phys. Chem.* **57**, 65 (2006).
12. C.-Y. Ruan, V. A. Lobastov, F. Vigliotti, S. Chen, A. H. Zewail, *Science* **304**, 80 (2004).
13. X. Zou, S. Hovmöller, *Acta Cryst. A* **64**, 149 (2008).
14. N. Gedik, D.-S. Yang, G. Logvenov, I. Bozovic, A. H. Zewail, *Science* **316**, 425 (2007).

15. F. Carbone, P. Baum, P. Rudolf, A. H. Zewail, *Phys. Rev. Lett.* **100**, 035501 (2008).
16. P. Baum, A. H. Zewail, *Proc. Natl. Acad. Sci. USA* **103**, 16105 (2006).
17. P. Baum, D. S. Yang, A. H. Zewail, *Science* **318**, 788 (2007).
18. G. M. Francis, L. Kuipers, J. R. A. Cleaver, R. E. Palmer, *J. Appl. Phys.* **79**, 2942 (1996).
19. M. C. Gordillo, J. Martí, *J. Chem. Phys.* **117**, 3425 (2002).
20. D. Argyris, N. R. Tummala, A. Striolo, D. R. Cole, *J. Phys. Chem. C* **112**, 13587 (2008).
21. P. L. Geissler, *J. Am. Chem. Soc.* **127**, 14930 (2005).
22. J. D. Smith *et al.*, *Proc. Natl. Acad. Sci. USA* **102**, 14171 (2005).
23. We also measured the ice dynamics at different graphite excitation fluences (11, 24 and 39 mJ/cm²), and the corresponding lattice expansions of the transient phase are 8.45%, 18.5% and 22.7%, respectively. The absence of a threshold, with a near linear dependence for ice mirrors the linearity found for the graphite substrate (39). However, at very high fluences, saturation of vibrational motions in highly excited HOPG would have to be considered (39).
24. K. Thürmer, N. C. Bartelt, *Phys. Rev. B* **77**, 195425 (2008).
25. J. Kubota, A. Wada, S. S. Kano, K. Domen, *Chem. Phys. Lett.* **377**, 217 (2003).
26. S. H. Garofalini, T. S. Mahadevan, S. Xu, G. W. Scherer, *Chemphyschem* **9**, 1997 (2008).
27. R. Rey, K. B. Møller, J. T. Hynes, *Chem. Rev.* **104**, 1915 (2004).
28. E. T. J. Nibbering, T. Elsaesser, *Chem. Rev.* **104**, 1887 (2004).
29. M. Schmeisser, H. Igley, A. Laubereau, *J. Phys. Chem. B* **111**, 11271 (2007).
30. A. P. Willard, D. Chandler, *J. Phys. Chem. B* **112**, 6187 (2008).

31. B. J. Gertner, J. T. Hynes, *Science* **271**, 1563 (1996).
32. P. Ball, *Chem. Rev.* **108**, 74 (2008).
33. A. D. Buckingham, J. E. Del Bene, S. A. C. McDowell, *Chem. Phys. Lett.* **463**, 1 (2008).
34. P. Jenniskens, D. F. Blake, *Science* **265**, 753 (1994).
35. P. Jenniskens, D. F. Blake, *Astrophys. J.* **473**, 1104 (1996).
36. L. Delzeit, D. F. Blake, *J. Geophys. Res.* **106**, 33371 (2001).
37. J. Steinbeck, G. Braunstein, M. S. Dresselhaus, T. Venkatesan, D. C. Jacobson, *J. Appl. Phys.* **58**, 4374 (1985).
38. A. B. Kuzmenko, E. van Heumen, F. Carbone, D. van der Marel, *Phys. Rev. Lett.* **100**, 117401 (2008).
39. R. K. Raman *et al.*, *Phys. Rev. Lett.* **101**, 077401 (2008).